ISSN: 0974-5823 Vol. 7 No. 4 April, 2022

International Journal of Mechanical Engineering

Interoperability IPT system accurate computation of MI between Spiral-Square Inductive Coupled Coils with Different Misalignments

Ravi Bukya* , B Mangu

[1,2] Dept. of Electrical Engineering, University College of Engineering, Osmania University,Telangana,India-07.

Abstract: In This Paper uses an analytical technique to determine the mutual inductance(MI) of two spiral square coils installed on a flat planar surface. The MI of the coils is calculated to account for any potential spacing changes.. In practice, spiral square coils are more tolerant of planar misalignments and, more critically, have a higher MI than, circular coils. However, whereas MI calculation methods for two spiral circular coils have been widely predictable, as well as a new modified Neumann's method, spiral square coils have received modest attention. Finite element analysis and an experimental setup are used to validate the results of Neumann's approach expected mutual inductance. Finally, the comparison is made between the three mutual inductance calculations: Neumann's approach, finite-element model, and Simulink result. In every case, the results of the three approaches are in good concurrence in MATLAB/SIMULINK.

Keywords : Electric Vehicle Charging, different compensation, electric vehicle, inductive power transfer, FEM analysis.

I. INTRODUCTION

In order to reduce emissions even more, we need to decrease our dependency on fossil fuels. Inevitably, power will exist. Because they run on renewable energy, electric vehicle (EV) no pollution. Because modern batteries are more energy efficient, electric vehicles is the best option[1]. The batteries in electric vehicles have a short lifespan and are expensive [2]. Charging options include wireless, inductive, and cable. Electric shocks or cable leaks in the rain or snow might occur if charging is inadequate. The grid and the load are intertwined. Compensation topologies, power electronics converters, and control methods are the other two major research areas in wireless charging systems. This measurement is known as mutual inductance (MI). The distance must be calculated when using wireless charging for electric vehicles [2-3]. Because high power and high switching frequency AC converter technology is now available, research into wireless charging systems (WCS) has flourished in recent years. [2-5] The advantages of implementing this technique.

This method can assist with power and environmentally friendly transportation [6-7]. Wireless Charging System (WCS) , as opposed to cable charging, allows you to reduce the size of the battery within EV. With this approach, the onboard battery may be kept to a minimum. The battery pack for an all-electric transport vehicle weighs about the same as one day's worth of food. Instead, it raises new questions about sustainability, ones that are creating debate in academia and the business community alike. WCS infrastructure is superior than saving batteries and boosting fuel efficiency.[8]

Developing an IPT system takes effort and time. It is possible to create high-efficiency compensation networks by combining compression networks and circuits [6-7], coil design approaches that allow for a large gap and misalignment tolerance, and compensation network interoperability processes. Improved coupling and power transfer are required, as is greater efficiency[8]. EV applications make use of a wide variety of compensating topologies. Primary and secondary coils are used to adjust capacitors. The comparable circuit of the system is detailed on pages[11-14]. To determine whether a scene is realistic, it can be replicated. Coil electromagnetics, on the other hand, makes use of the electromagnetic fields produced by coils. Simulating the electromagnetic properties of the coil is not a possibility due to their complexity. The process is repeated if the results are unsatisfactory.

Hybrid compensation topologies using P-S compensation did not have a single similarity. WPT was developed by combining an inductor, capacitor, and Inductor-Capacitor-Inductor (LCL). These networks can be seen on both the transmitter and receiver sides of the [2-5]. As a result, resonance frequency is unaffected by coupling or load. The supplementary inductances in these topologies are as large as or larger than the primary inductances. LCC might be corrected on both sides by using additional inductors with lower total inductances than the primary coil. It has two rotating axes, like LCL or CLCL topologies.

The Inductive Power Transfer(IPT) technology maximizes power transmission by reducing the volt-ampere rating. For many years, scientists have examined the effects of IPT capacitor compensation. compensation topologies are formalized by Covic and colleagues (2013) (2016). Four contactless compensation topologies were studied by Rena Ezhil in 2015. Compressors and

capacitors with a two-sided charging compensator (2014, 2016). Both Li et al. 2017 and Matsumoto et al. 2011 created compensating topologies that were dual-sided (LC and CC). (Matsumoto and colleagues) It is possible that the techniques of Mohamed, Qu, and Zhang might improve IPT misalignment tolerance. The simplest compensatory topology to use is S/S. In order to achieve high resonant IPT efficiency, both the transmitter and receiver must be equipped with a control mechanism. Multiple IPT control and optimization strategies may be found in the scientific literature. Their high-frequency inverter controller makes use of a fuzzy logic algorithm that is evolutionary in nature (Wang et al., 2015).

Maintain the same voltage or current when charging the batteries. There is a lateral misalignment in the MRC WPT system, according to Zhigang Dang (HER). A review of the literature by Diekhans and De Doncker (2015a), Bowkett et al (2015). The year is 2016 (or later) (2015). Prasanna and co-authors (2017). It's tough to put together a boost or buck converter that also has a rectifier circuit. For instance, take Maddalena et al. as an example (2016). “Wireless e-bike battery charging improves efficiency while also tracking the amount of power used. Both the transmitter and receiver are required to control voltage and current in order to produce a functional IPT system”. The efficiency, current, and voltage are affected by the coils' coefficient of coupling when they are poorly linked (k). The double-sided LCCL resonant network is described by Shenqin Yang (2018). (ICPT). According to his results, there was an increase in the coil's magnetic field and induction voltage, as well as a decrease in inductance. The Hon. Koufos Koufos (2020). A scale model of a transformer, in the form of a circle.

An examination of interoperability The wireless charging interoperability research is critical [1–44]. The word "interoperability" refers to the ability of a transmitter (off-load) system and a receiver (on-board) system that were independently built by different manufacturers to operate together and ensure battery charging to be understood properly. The connection mechanism in the aforementioned project is built using several power pads [42]. The objective is to see how well various systems integrate, a combination of two of the three power pads is used. In this article, four interoperability setups are compared and compared.

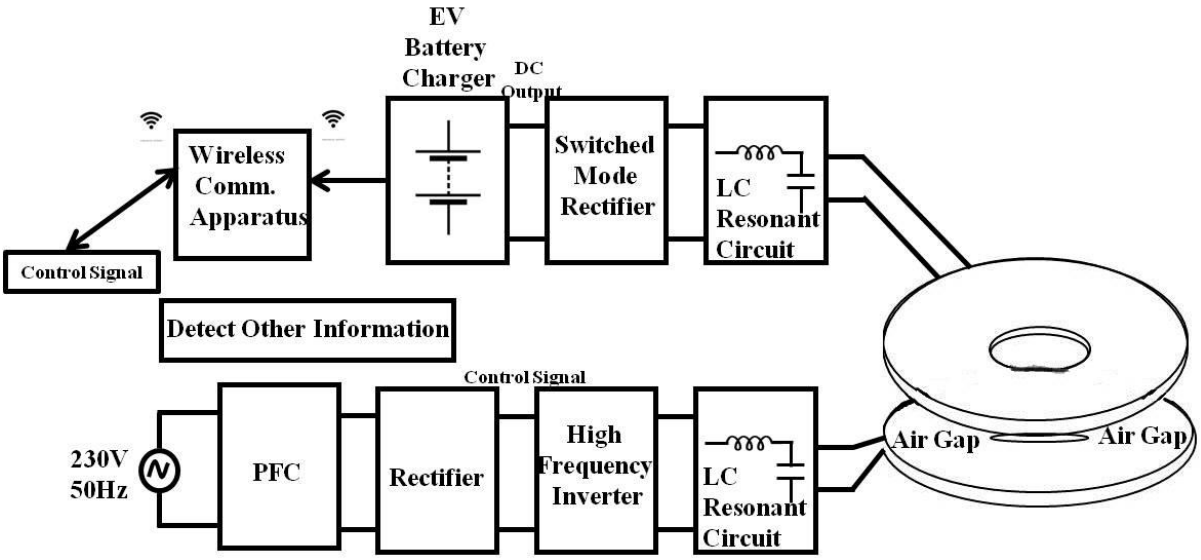

Figure.1. Schematic representation of parallel/series resonant WPT system

An electric car battery charging system using a parallel/series resonant WPT is designed and analysed in this study. For battery charging, a DC-DC buck converter with a closed loop on the receiver side is used. Figure 1 depicts a simple schematic design of the system. There are two sections to this document: Section 2 presents a simple mathematical description of the parallel/series resonant WPT system. Section 3 goes into detail about the simulated components. Detailed findings and comments on how the implementation went may be found in Section 4. Section 5 concludes the paper by presenting the findings and conclusions.

II. Analysis and Modelling of Current-fed Wireless Inductive Power Transfer System

Nikola Tesla created resonant antennae power transfer (RAPT), which was later patented by MIT and Intel. This technique's core ideas are similar to those of IPT. Because of the use of high-quality factor coils and a high operating frequency, the air gap length is significantly longer than with an IPT system. A range of up to 10 meters is achievable with a frequency of operation in the MHz band. However, for a few kW of power transmission suited for EV applications with an air gap, this RAPT technology is virtually as good as the IPT system.. The transmission of power capability for a VA rating was proven by this technique's predicted power input to the load. To compensate for leakage inductance and avoid reactive current from rising due to losses, high compensation networks are coupled. Figure 8 depicts a typical WPT current-fed converter with parallel resonance for lower circulating currents.

Because of the parallel capacitors, the circulating current path has a low impedance. Voltage stress rises as a result of power transmission.

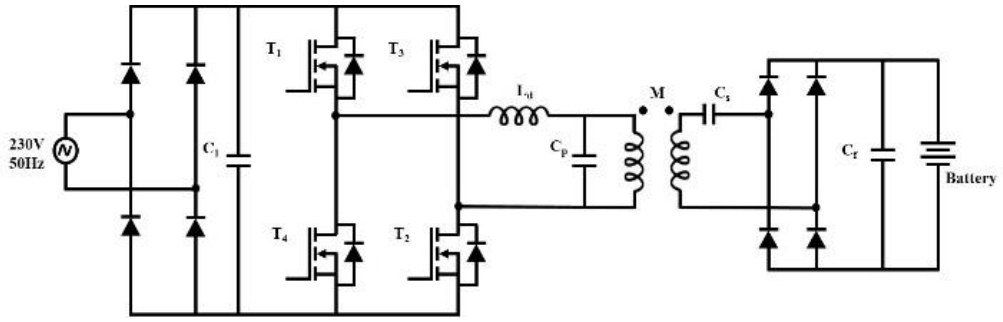

Figure.2. : An inductive power transfer system.

The advantages of each of these topologies differ. Because of its low VA rating, constant voltage and current no matter how much power is being drawn from it, high misalignment tolerance, bifurcation tolerance, and great efficiency, it's ideal for low-power applications. Figure.2. depicts the basic equivalent circuit layout for a current-fed compensation network using a mutual inductance model. This article makes use of the P-S Compensation topology for researcher analysis.

A. Modelling of the P-S Compensation Topology

The transmitter voltage,

$$\bar{V}_1 = \bar{I}_1 r_1 + jw\ L_1\ \bar{I}_1 - jw\ M\ \bar{I}_2 \qquad \text{.....(2.6)}$$

$$jw\ M\ \bar{I}_1 = jw\ L_2\ \bar{I}_2 + R_L \bar{I}_2 \qquad \text{.....(2.7)}$$

Transmitting and receiving coil currents,

$$\bar{I}_2 = \frac{jw\ M\ \bar{I}_1}{jw\ L_2 + r_2 + R_L} = \frac{jw\ M\ \bar{I}_1}{Z_2} \qquad \text{.....(2.8)}$$

The equivalent impedance receiving side(Z_2), Equation (2.9) in (2.6),

$$\bar{V}_1 = r_1\ \bar{I}_1 + jw\ L_1\ \bar{I}_1 + \frac{\omega^2\ M^2}{Z_2} \qquad \text{.....(2.9)}$$

Total Impedance (Z_t) from transmitting coil,

$$Z_t = r_1 \bar{I}_1 + j\omega\ L_1 + \frac{\omega^2\ M^2}{Z_2} \qquad \text{.....(2.10)}$$

Reflected impedance,(Z_r),

$$Z_r = \frac{w^2 M^2}{Z_2} \qquad \text{.....(2.11)}$$

Equation (2.2) and (2.6)

$$k = \frac{M}{\sqrt{L_1 L_2}} \qquad \text{.....(2.12)}$$

$$\frac{\bar{I}_2}{\bar{I}_1} = \frac{jw\ M}{R_L + r_2 + jw\ L_2} \qquad \text{.....(2.13)}$$

There is an equation for inductive power transfer efficiency and maximal power transfer. (2.14) and (2.15).

$$\eta = \frac{\left|\bar{I}_2\right|^2 R_L}{\left|\bar{I}_1\right|^2 \mathrm{Re}\{Z_t\}} = \frac{R_L}{r_1 \frac{L_2{}^2}{M^2} + (R_2 + r_2)\left[1 + \frac{r_1 (R_L + r_2)}{w^2 + M^2}\right]} \qquad \text{.....(2.14)}$$

$$P_{L,max} = \frac{1}{2}\frac{(\omega\ M\ I_1)^2}{\omega L_2} \qquad .....(2.15)$$

The mutual inductance of a system was determined using current-fed compensation by the researchers. Because of the impedance transfer, a current-fed system has a high efficiency, a large load variation, and a low mutual inductance with a high power factor . Zero coupling is not enabled in a load due to the higher inverter device voltage, however it is in a voltage source due to the higher inverter device voltage. To maintain voltage fluctuations to a minimal, a current input is required.

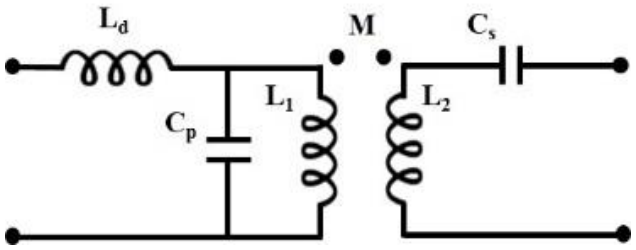

Figure.3. P-S compensation circuit.

III. GENERAL POSSIBLE VARIATION OF SPIRAL-SQUARE COIL

A. Basic Possible variation possibilities

In this paper, MI were compute accurately is the mainly analyzed. MI between spiral-square coils is investigated; coils were placed on a flat planar surface that coincided in space. If the coils position is change than the MI of the coils is fluctuates with variation in, different variations of coils thoroughly analyzed in this paper. Types of possible variation as shown in figure.2. and its corresponding schematics are shown in figure.3. The parameters for used in this work were described in table. I.

Table- I: Calculated Parameters

Parameters	**Theoretical Calculation**	**Practical**
Source Current, (I_d)	10A	10.5A
Primary and Secondary Inductance, (L_1,L_2)	150µH 180 µH	150µH 180 µH
Mutual Inductance, (M)	110 µH	120 µH
Primary and Secondary Capacitance, (C_1,C_2)	250µF 280 µF	250µF 280 µF
Resonating capacitor, Inductor (C_r ,L_r)	320 µF, 150 µH	320 µF, 150 µH
Inverter switching frequency,(f_ω)	80kHZ	80kHZ
Coil turns ratio,(N)	1:1	1:1
Output voltage ,(V_o)	48V	48V
Output Current, (I_o)	10A	12A
Efficiency, (η)	93.5	93.6
Cost	Low	High
Power Loss	Low	High

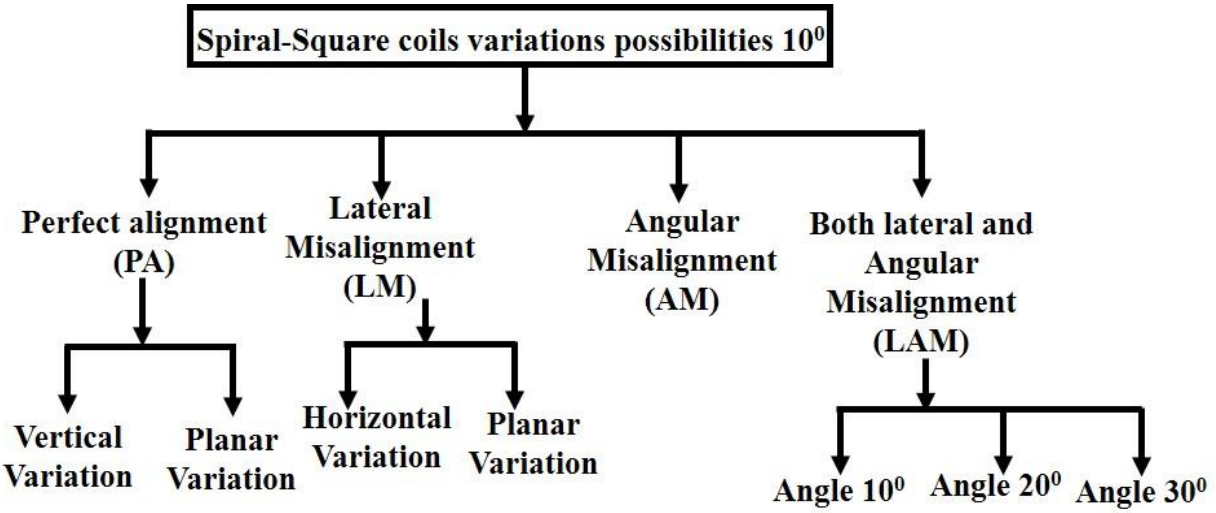

Figure.4. Spiral-square coil possible variations.

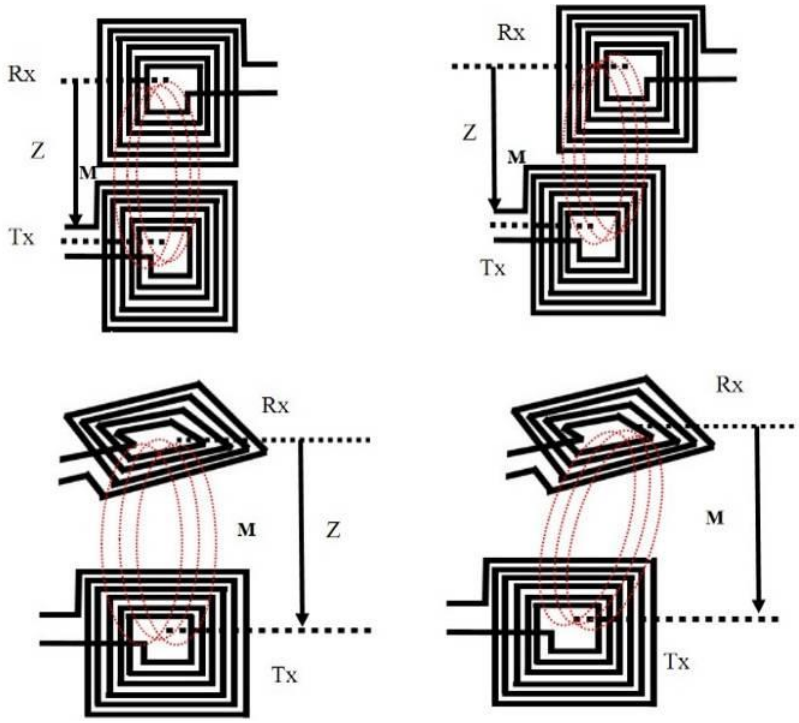

Figure.5. Examined Square coils different variations.

Shows the coil characteristics used in this research study. Perfect alignment refers to a coil arrangement where the PC and SC are aligned on a level plane (PA). In this case, vertical and planar modifications are explored Figure. 3. This occurs when PC and SC are properly aligned and coils are closely spaced. As PC moves away from SC, the coil coupling changes. SC and PC are arranged in a planar variant, and PC is rotated around its axis at various angles (Figure. 3). (b). Keeping the coil spacing constant keeps the coil overlap area constant, so the flux linkage variation is minimal. On real-time systems, lateral misalignment occurs when coils are set in a parallel plane but are moved horizontally (LM)[4]. In this case, the coils' axes are misaligned. As shown in Figure. 3, LM fluctuates horizontally and laterally . The flux linkage and MI of the coils drop as the PC moves away from the SC[1]. A PC can also be angled up or down (0-90) due to uneven surface impacts; this is called angular misalignment. The equivalent circuit as shown in figure.4. In this primary coils as PC and Secondary coil as SC in between coupling coils as connected so, that source and output load to calculate by using equivalent circuit.

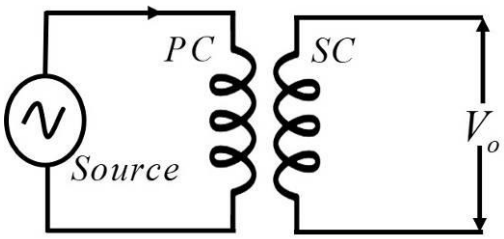

Figure.6. Inductive coil equivalent model.

Figure. 7. Similar to lateral and angular misalignments, SC can be tilted and altered horizontally, as seen in Figure. 5. The tilted angle and the horizontal distance effect MI in this misalignment situation. The above-mentioned misalignments are estimated analytically and validated experimentally. The results and comparisons are discussed in the following sections.

Table- II: Angular Misalignment

Parameter	Descriptions
PC,SC	Primary Coil, Secondary Coil
h	Coil Hight in diameter
d	Coil distance
Ɵ	Angle between PC and SC

B. Square structure

For planar spiral square coil inductance were simple modification of the wheeler formula can be expressed as follows shown in figure.5 is represented as spiral square coil structure with multi coil system.

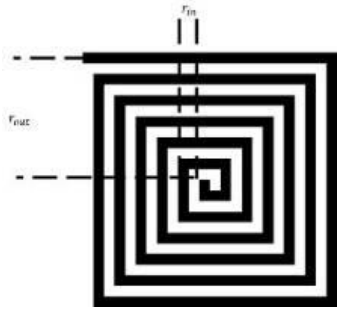

Figure.7. Representation of a spiral square coil.

$$L_{sq} = \frac{2\mu N^2 P}{\pi}\left(\ln\left(\frac{2.067}{Q}\right) + 0.17Q + 0.125Q^2\right) \quad .....(3.1)$$

Where

N =Number of Turns

$$P = \frac{1}{2}\left(r_{out} + r_{in}\right), \quad Q = \frac{\left(r_{out} + r_{in}\right)}{\left(r_{out} + r_{in}\right)} \quad .....(3.2)$$

IV. ANALYTICAL COMPUTATION OF MI BETWEEN IDENTICAL SPIRAL SQUARE INDUCTIVE COILS

The misalignments of spiral square coils, which are the same as spiral circular coils, are presented in the following sections, and analytical calculations are only done for the circular coil misalignments indicated. The area of a square coil with a diameter equal to that of a spiral circular coil. is 4/π times higher. As a result, using the equation below, the MI between the planar spiral square coil can be computed. (4).

$$M_{nj}\left(sqare\right) = \left(\frac{4}{\pi}\right)^2 M_{nj}\left(cir\right) \quad .....(4.1)$$

Figure. 7. illustrates a precisely aligned array of spiral square coils with many turns. The mutual inductance may be calculated using the formula below.

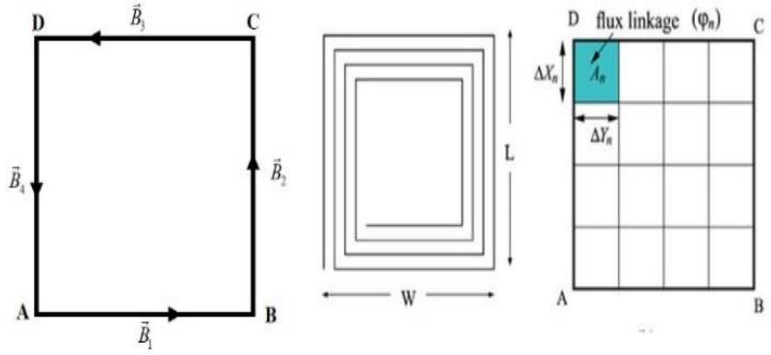

Figure.8. Spiral-Square coil (a) single turn (b) Segmented turn (c) Double turn

$$M = \left(\frac{4}{\pi}\right)^2 \sum_{n=1}^{N_1}\sum_{j=1}^{N_2} \frac{\mu_o \pi {a_n}^2 {b_j}^2}{2\left(z^2 + {a_n}^2 + {b_j}^2\right)^{\frac{3}{2}}} \qquad .....(4.2)$$

Where ai, bj represents the spiral circular transmitter and receiver coils i^{th} and j^{th} turns radius respectively and calculation of these parameters are presented in Eq. (4).

$$M = \left(\frac{4}{\pi}\right)^2 \left\{ \sum_{n=1}^{N_1}\sum_{j=1}^{N_2} \frac{\mu_o \pi {a_n}^2 {b_j}^2}{2\left(z^2 + {a_n}^2 + {b_j}^2\right)^{\frac{3}{2}}} + \sum_{k=1}^{p}\sum_{m=1}^{q} \frac{\mu_o \pi {a_k}^2 {b_m}^2}{2\left(z^2 + {a_k}^2 + {b_m}^2\right)^{\frac{3}{2}}} \right\}$$

$$M = \left(\frac{4}{\pi}\right)^2 \sum_{n=1}^{N_1}\sum_{j=1}^{N_2} \frac{\mu_o \pi {a_n}^2 {b_j}^2}{2\left(z^2 + {a_n}^2 + {b_j}^2\right)^{\frac{3}{2}}} \qquad .....(4.3)$$

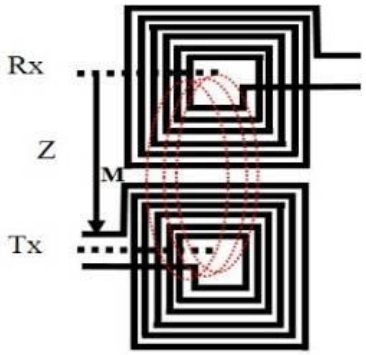

Figure.9.Multi turn spiral square coupled coils at Perfect Alignment.

A. Planar Misalignment MI Calculation

Figure. 8. illustrates a planar misalignment of the spiral square coil's transmitter and reception coils. The expression for computation of MI is given in Eq. (6).

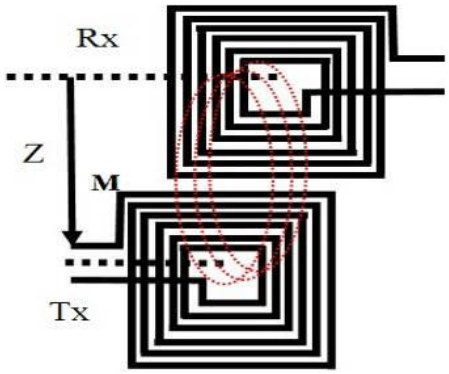

Figure.10. Multi turn spiral square coupled coils at Planar Misalignment.

$$M=\left(\frac{4}{\pi}\right)^2\left\{\sum_{n=1}^{N_1}\sum_{j=1}^{N_2}\frac{\mu_o\pi a_n{}^2 b_j{}^2}{2\left(z^2+a_n{}^2+b_j{}^2\right)^{\frac{3}{2}}}+\sum_{k=1}^{p}\sum_{m=1}^{q}\frac{\mu_o\pi a_k{}^2 b_m{}^2}{2\left(z^2+a_k{}^2+b_m{}^2\right)^{\frac{3}{2}}}\right\} \quad .....(4.3)$$

Where a_i, b_j and a_k, b_l represents radius of the perfectly aligned and misaligned turns of spiral circular transmitter and receiver coils respectively and calculation of these parameters are presented in Eq. (6) Investigation'.

B. Angular Misalignment MI calculation

Any one The angular misalignment of the spiral square coupled coils is shown in Figure. 9. The mutual inductance can be computed by using Eq. (7).

$$M=\left(\frac{4}{\pi}\right)^2\sum_{n=1}^{N_1}\sum_{j=1}^{N_2}\frac{\mu_o\pi a_n{}^2 b_j{}^2}{2\left(z^2+a_n{}^2+b_j{}^2\right)^{\frac{3}{2}}} \quad .....(4.4)$$

Where

$$Z_{avg}=\frac{Z_1+Z_2+Z_3}{3}$$

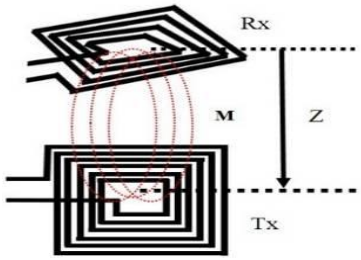

Figure.11. Multi turn spiral square coupled coils at Planar Misalignment.

C. Planar and Angular Misalignment MI calculation

Fig. 9. illustrates a planar and angular mismatch of the spiral square coil's transmitter and reception coils. The mutual inductance can be calculated using Eq. (4.5).

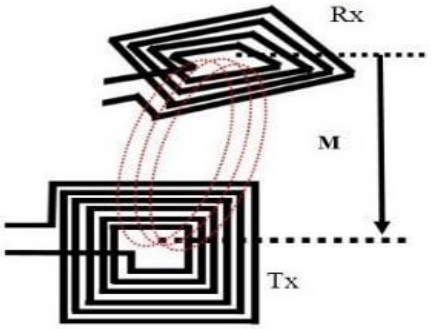

Figure.12. Multi turn spiral square coupled coils at Planar and Angular Misalignment.

$$Z_{avg} = \frac{Z_1 + Z_2 + Z_3}{3}$$

$$M = \left(\frac{4}{\pi}\right)^2 \left\{ \sum_{n=1}^{N_1} \sum_{j=1}^{N_2} \frac{\mu_o \pi a_n^{\,2} b_j^{\,2}}{2\left(z^2 + a_n^{\,2} + b_j^{\,2}\right)^{\frac{3}{2}}} + \sum_{k=1}^{p} \sum_{m=1}^{q} \frac{\mu_o \pi a_k^{\,2} b_m^{\,2}}{2\left(z^2 + a_k^{\,2} + b_m^{\,2}\right)^{\frac{3}{2}}} \right\} \quad .....(4.5)$$

The aforementioned equation can be applied to any spiral square coils, although it is recommended that the computation be done first for spiral circular coils. As a result, all analytical calculations for spiral square coils are limited to the misalignments described.

V. COMUTATION OF MI USING FEM

The analytically determined mutual inductance between the spiral square connected coils was validated using the 3-D finite element modelling (FEM) Programme ANSYS. The two linked coils' circuit topology PC and SC are inductively linked transformers, as illustrated in the corresponding circuit diagram, with PC connected to the power supply and SC connected to the secondary side coil in figure.14.

Table- III: Angular Misalignment

Angle(Θ)	**Angular Misalignment**			
	FEM(µH)	**Analytical(µH)**	**Practical**	
			Degree	
0	2.60	2.60	0	2.35
10	2.65	2.65	10	2.40
20	2.69	2.69	30	2.49
30	2.82	2.82	40	2.70
40	2.94	2.94	50	2.74
50	3.05	3.05	70	2.54
60	3.01	3.01	90	1.06
70	2.56	2.56	-	-
80	1.79	1.79	-	-
90	0.78	0.80	-	-

Table- IV: Angular and planar Misalignment

Angle(Θ)	**Angular and planar Misalignment**			
	FEM(µH)	**Analytical(µH)**	**Practical**	
			Degree	
0	12.60	12.60	0	12.35
1.3	12.65	12.65	1.3	11.40
2.3	11.69	11.69	2.3	10.49
3.3	10.82	10.82	3.3	9.70
4.3	10.94	9.94	4.3	8.74
5.3	9.05	8.05	5.3	7.54
6.3	9.01	7.01	6.3	6.06
7.3	8.56	6.56	-	-
8.3	7.79	5.79	-	-
9.3	6.78	4.80	-	-

Maxwell 14.0.0. Figures 12. and 13. illustrate the spiral square coil setups created in the FEM simulation without a core, as well as those with a core and chassis.

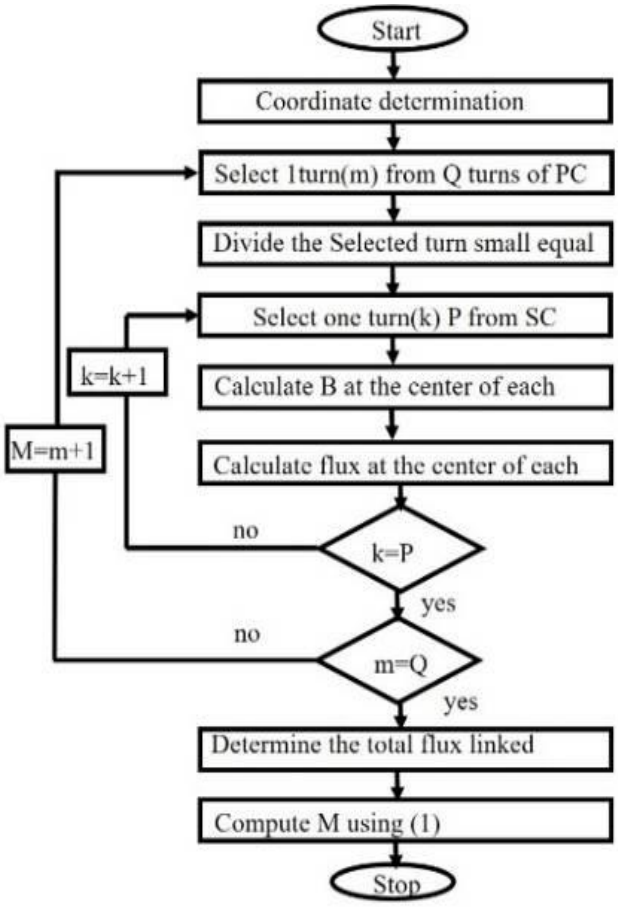

Figure.13. Flowchart describing the numerical evaluation.

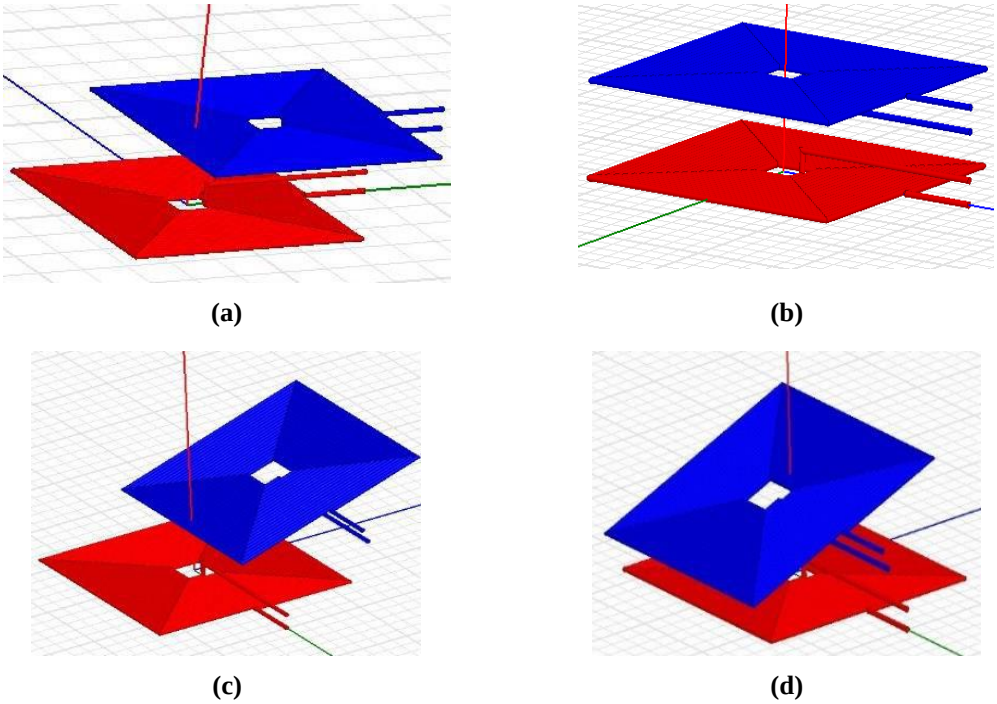

(a) **(b)**

(c) **(d)**

Figure.14. Simulated Square Coils Setup using FEM (a) Perfect Alignment, (b) Planar Misalignment (c) Angular Misalignment (d) Planar & Angular Misalignment.

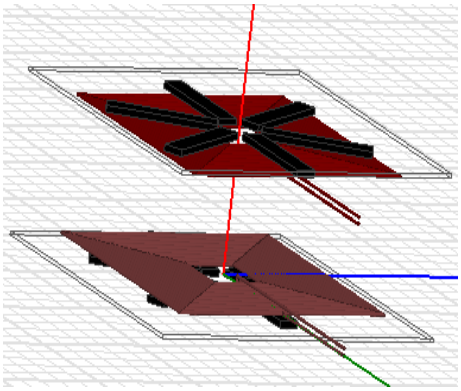

Figure. 15.Spiral Square Coil setups with core and chassis developed in FEM.

The Figure. 14. The flux density pattern between the spiral square inductively linked coils at 100 mm spacing under various misalignment situations is depicted. As the receiver coil moves away from the transmitter coil, the flux connections weaken, resulting in a decrease in mutual inductance.

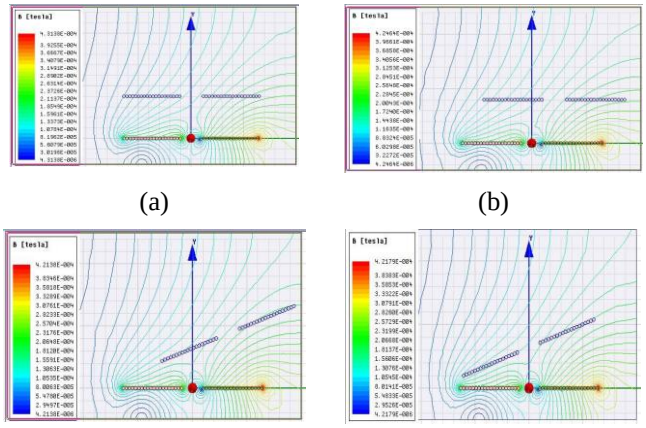

(a) (b)

(c) (d)

Figure.16. Magnetic flux density distribution without a magnetic core between connected coils at a distance of 100 mm, (a) Perfect Alignment, (b) 80 mm Planar Misalignment, (c) 300 Angular Misalignment, (d) 80 mm Planar & 150 Angular Misalignment.

The magnetic flux density distribution between the coupled coils with core and chassis are shown in Figure. 15. structures. From the Fig. 15.(b) it is clear that the maximum value of flux linkages will reduce compared to the ferrite core because the chassis i.e., steel cover will dismisses the magnetic field.

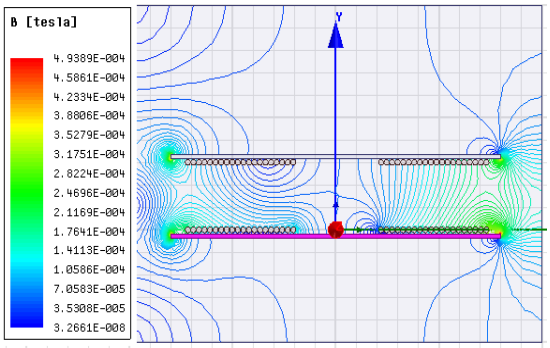

(a)

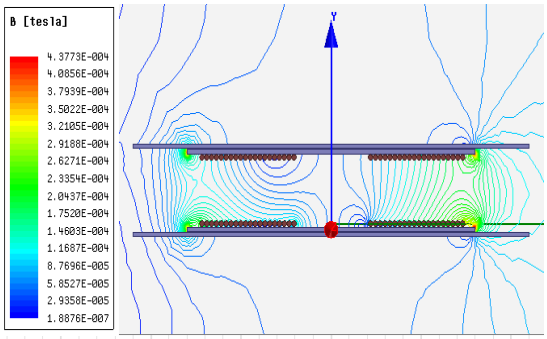

(b)

Figure. 17. Magnetic flux density distribution between the identical square coupled coils at 100 mm distance with Perfect Alignment, (a) With core, (b) With core and chassis.

VI. ANALYSIS AND DISCUSSION OF NUMERICAL RESULTS

The figures Experimental setting, analytical technique, and finite element model the numerical outcomes of the three analyses are shown. in Table IV, while Figures. Researchers have made several general comparisons, which are included below. Horizontal variation at Maximum and minimum are 11.4 cm and 0 cm. Rotational variation is 90° max. Because the MI value is repeatable for square geometry. We observe that with this 1cm increased in horizontal and vertical. The experimental readings are recorded at a step of 15 change due to practical constraints. Variation in Vertical and Planar Alignment. To Compared properly aligned are summarized in , See Table IV for vertical and planar versions. 13.14 Figures.

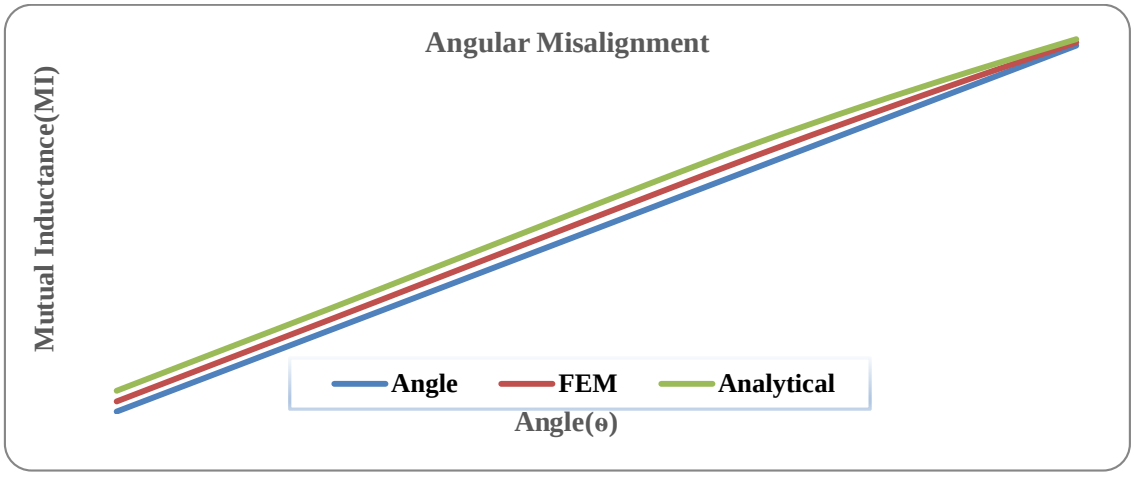

Figure. 18. Lateral misalignment—Horizontal variation.

Angular Misalignment The numerical results for all four investigations for angular analytical with practical and angular FEA with different angle variations' has shown in figure 16. The MI is various compare with theoretical to practical the theoretical value is some various with practical MI seen in figure.

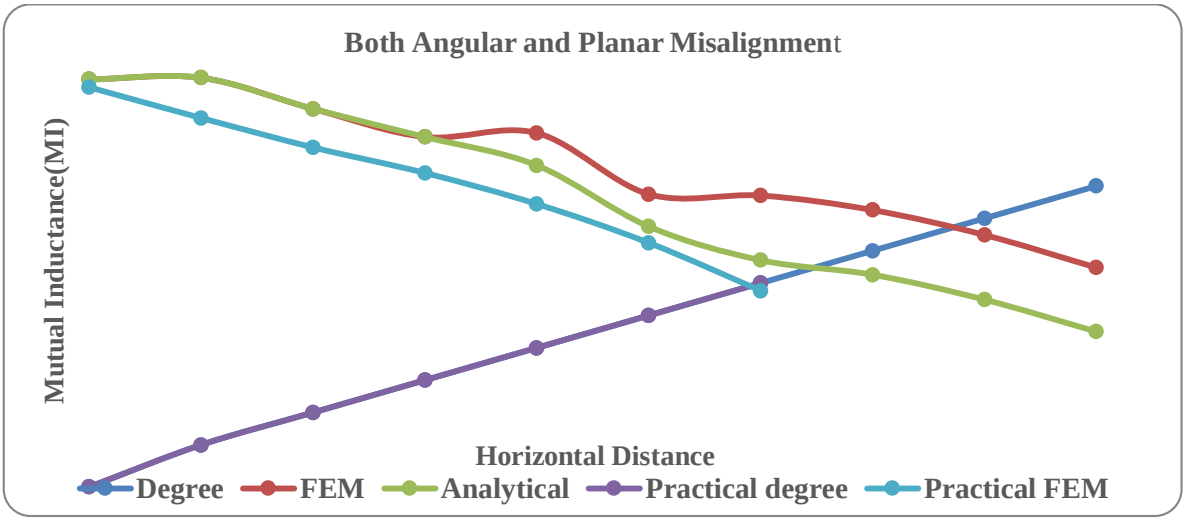

Figure. 19. Misalignment on both the lateral and angular planes (10^0 , 20^0 , 30^0).

Lateral Misalignment Variations on a Horizontal and Planar Scale This section presents and compares the numerical findings from all three studies on situations of horizontal and planar variation that are laterally misaligned.

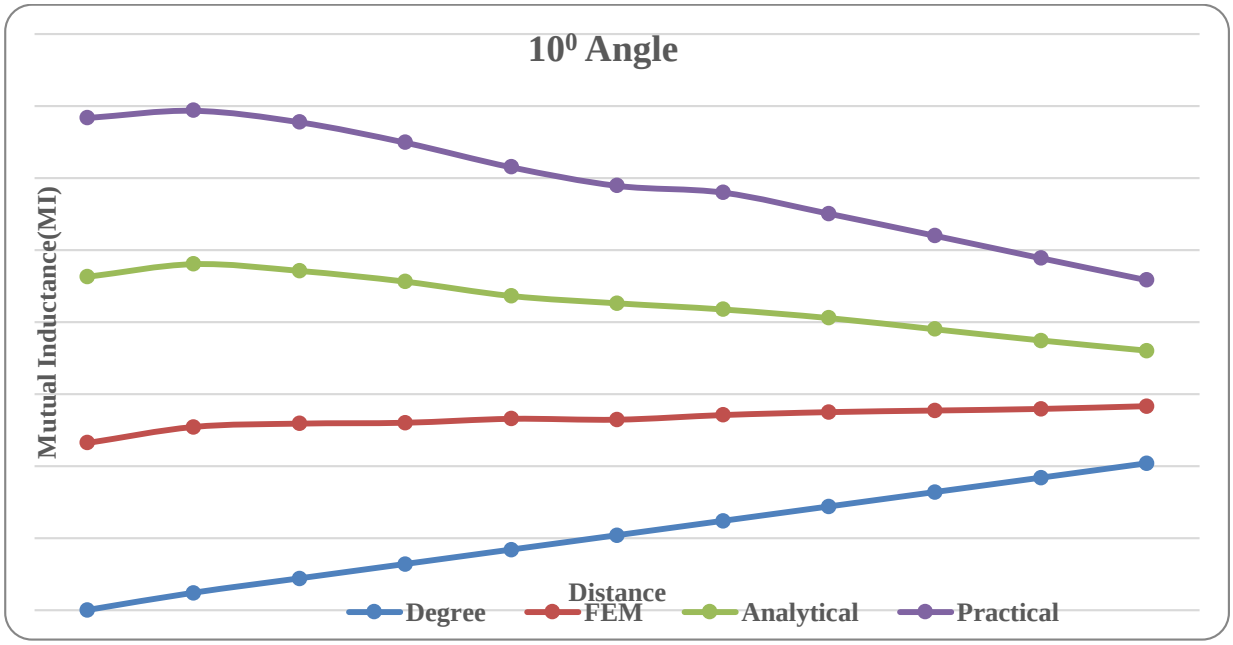

Figure. 20. Misalignment on both the lateral and angular planes (10^0 , 20^0 , 30^0).

Table- IV: Angular and planar Misalignment

10^0 Angle				**20^0 Angle**			
Distance(cm)	**FEA (µH)**	**Analytical (µH)**	**Practical (µH)**	**Angle^0(degree)**	**FEA (µH)**	**Analytical (µH)**	**Practical**
0	11.62	11.54	11.03	0	8.15	8.32	8.25
1.2	11.52	11.32	10.65	1.6	7.95	7.98	8.16
2.2	10.75	10.62	10.32	2.6	7.65	7.52	7.90
3.2	9.81	9.81	9.65	3.6	6.96	6.96	7.50
4.2	9.08	8.54	8.94	4.6	6.65	6.32	6.85
5.2	8.02	8.09	8.16	5.6	5.76	5.78	6.30
6.2	7.34	7.34	8.12	6.6	5.17	5.19	5.69
7.2	6.54	6.54	7.25	7.6	4.56	4.59	5.02
8.2	5.65	5.65	6.50	8.6	3.96	3.96	4.45
9.2	4.76	4.76	5.72	9.6	3.26	3.26	3.69
10.2	3.95	3.86	4.90	10.6	2.65	2.65	3.05

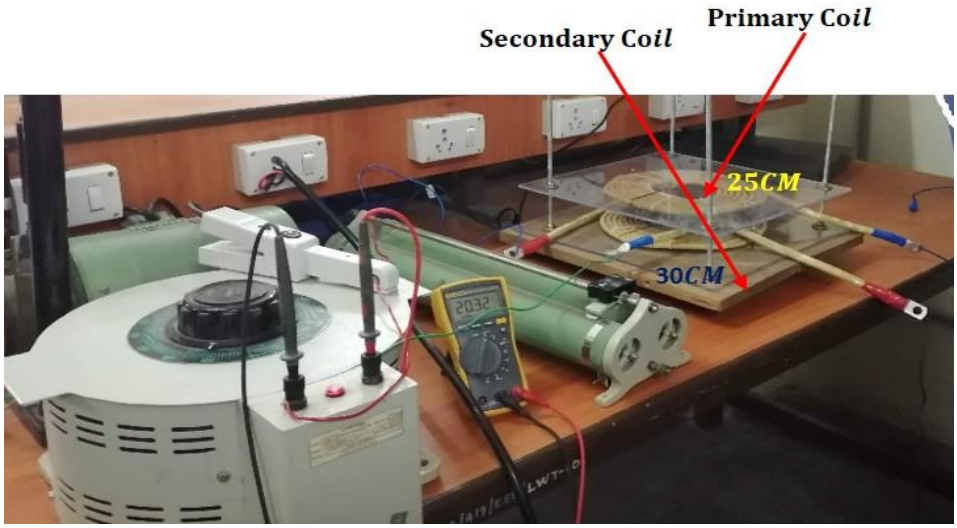

Figure.21. Expermental MI Investigation setup

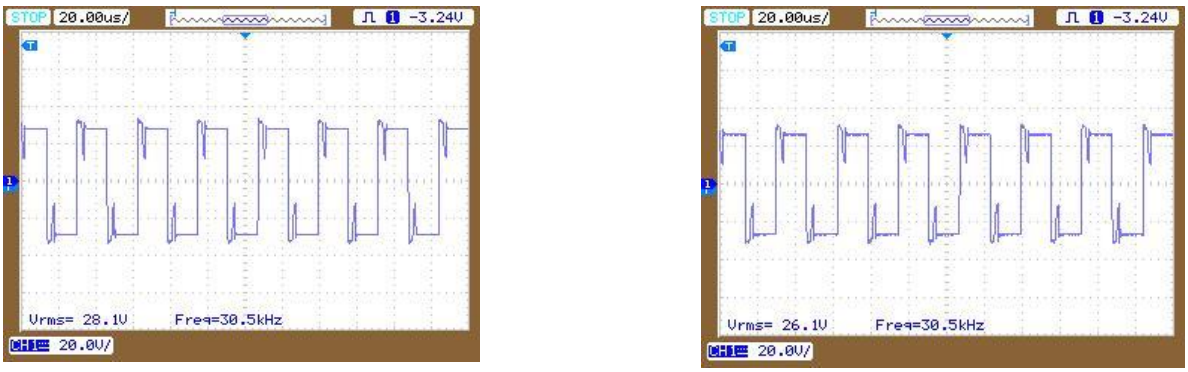

(a) (b)

Figure.22. Receiver open circuit voltages at 100 mm distance for identical spiral square coils, (a) Perfect Alignment, (b) 80 mm Planar & 150 Angular Misalignment.

RESULT AND DISCUSSION

MI is calculated using a spiral square coil model. The information Neumann's method, which is based on the Biot-Savart law, is used to compute the MI between two air core square coils. The types and variations of misalignment are investigated. The analysis contrasts the results of the analytical, FEA, and experimental methods. The coupling and MI between coils reduces as the distance between them increases. The experimental and FEA results are very close, with a margin of error of less than 10%. The study's findings are as follows.

- High coil spacing and large horizontal and vertical misalignments have little impact on MI. This shows little coupling in CET systems and no power transmission.
- Planar variation has little impact on MI. Variations in system power transfer are unchanged.
- Angular misalignment moves half of the coil closer to the EC perimeter, boosting MI values, while other angles reduce MI values. System variations cause instability.

APPENDIX

A. Calculations

The examples below examine the calculation technique in depth to verify the proposed analytical strategy for calculating mutual inductance. Consider two 18 cm long and 18 cm wide square coils with a conductor diameter of 1.83mm. The PC and SC coils have 11 and 9 turns, respectively. The PC's current flow is 10 A. The following variants were chosen to illustrate the analytical model.

1) Case I: SC maintained a vertical height of 2 cm above EC. Perfect Alignment—Vertical Variation: SC maintained a vertical height of 2 cm above EC.

2) Case II: SC was held vertically at 2.1 cm and rotated at a 10 degree angle to achieve perfect alignment.

3) Case III: Angular Misalignment: The distance between SC and EC is 12.8 cm from Centre. SC is 10 degrees away from PC.

ACKNOWLEDGMENT

Thank You to MoTA, The Indian Government, also grace full to Osmania University, and Electrical Engineering Department.

REFERENCES

1. G. A. Covic, and J. T. Boys, "Inductive power transfer," Proceedings of the IEEE , vol.101, no.6, pp.1276,1289, June 2013.
2. A. Kurs, A. Karalis, R. Moffatt, J. D. Joannopoulos, P. Fisher, and M. Soljacic, "Wireless power transfer via strongly coupled magnetic resonances," Science, Vol. 317, 83-86, 2007.
3. F. Musavi, and W. Eberle, "Overview of wireless power transfer technologies for electric vehicle battery charging," Power Electronics, IET , vol.7, no.1, pp.60,66, January 201, vol.61, no.5, pp.2307,2315, May 2014.
4. Ravi Bukya, Mangu, A.Jayaprakash and Jatoth Ramesh " A Study on Current-fed Topology for Wireless Resonant Inductive Power Transfer Battery Charging System of Electric Vehicle" PARC-2020, feb-28-29,vol.1,pp May-2020.
5. A. Khaligh and S. Dusmez, "Comprehensive Topological Analysis of Conductive and Inductive Charging Solutions for Plug-In Electric Vehicles," in IEEE Transactions on Vehicular Technology, vol. 61, no. 8, pp. 3475-3489, Oct. 2012.
6. D. Patil, M. Ditsworth, J. Pacheco and W. Cai, "A magnetically enhanced wireless power transfer system for compensation of misalignment in mobile charging platforms," IEEE ECCE, 2015, pp. 1286-1293.
7. C. J. Kaufman, Rocky Mountain Research Lab., Boulder, CO, private communication, May 1995.
8. D. Patil, Marco Sirico, Lei Gu, Babak Fahimi Patil, M. Sirico, L. Gu and B. Fahimi, " Maximum efficiency tracking in wireless power transfer for battery charger: Phase shift and frequency control", Proc. IEEE Energy Conversion Congress and Exposition (ECCE), 18-22 Sept. 2016, Milwaukee, WI, USA.
9. B. Mangu, S. Akshatha, D. Suryanarayana and B. G. Fernandes, "Grid-Connected PVWind-Battery based Multi-Input Transformer Coupled Bidirectional DC-DC Converter for household Applications," IEEE Trans. Emerg. Sel. Topics Power Electron., vol. 4, no.3, Sept. 2016.
10. Y. Yorozu, M. Hirano, K. Oka, and Y. Tagawa, "Electron spectroscopy studies on magneto-optical media and plastic substrate interfaces(Translation Journals style)," IEEE Transl. J. Magn.Jpn., vol. 2, Aug. 1987, pp. 740–741 [Dig. 9th Annu. Conf. Magnetics Japan, 1982, p. 301].
11. Pradipta Patra, Susovon Samanta, Amit Patra, Souvik Chattopadhyay, "A Novel Control Technique for Single-Inductor Multiple-Output DC-DC Buck Converters", IEEE International Conference on Industrial Technology, Mumbai, India, 15-17 Dec. 2006.
12. S. Samanta, A.K. Rathore, Sanjib Kumar Sahoo, "Current-fed full-bridge and half-bridge topologies with CCL transmitter and LC receiver tanks for wireless inductive power transfer application", IEEE Region 10 Conference (TENCON), Singapore, 22-25 Nov. 2016.
13. V.R. kiran, R.K Keshri, Manuele Bertoluzzo, "Efficient Wireless Charging of Batteries With Controlled Temperature and Asymmetrical Coil Coupling" IEEE International Conference on Power Electronics, Drives and Energy Systems (PEDES), Chennai, India, 18-21 Dec. 2018.
14. Y. Guo; Y Zhang, B. Yan, Ke Wang, Z Zhang, Lifang Wang "Interoperability Analysis of Compensation Network in Electric Vehicle Wireless Charging System" 2018 IEEE International Power Electronics and Application Conference and Exposition (PEAC), Shenzhen, China, 27 December 2018.